

## Solar chimney optimization for enhancing thermal comfort in Egypt: An experimental and numerical study



Ahmed Abdeen<sup>a,b,\*</sup>, Ahmed A. Serageldin<sup>c</sup>, Mona G.E. Ibrahim<sup>a</sup>, Abbas El-Zafarany<sup>d</sup>, Shinichi Ookawara<sup>e</sup>, Ryo Murata<sup>e</sup>

<sup>a</sup> Energy Resources Engineering Department, Egypt-Japan University of Science and Technology, Alexandria, Egypt

<sup>b</sup> Architecture Engineering Department, Assiut University, Egypt

<sup>c</sup> Shoubra Faculty of Engineering, Benha University, Egypt

<sup>d</sup> Department of Urban Design Egypt, Cairo University, Cairo, Egypt

<sup>e</sup> Tokyo Institute of Technology, Tokyo, Japan

### ARTICLE INFO

#### Keywords:

Solar chimney  
Thermal comfort  
Natural ventilation  
CFD simulation  
Optimization

### ABSTRACT

Air motion can be induced in naturally ventilated buildings using passive solar chimneys. This work aimed to optimize solar chimney design to maximize indoor air velocity induced by natural convection, with a particular emphasis on thermal comfort. A three-dimensional, quasi-steady computational fluid dynamics (CFD) model was established for the prediction of buoyant air flow using the renormalization group (RNG)  $k-\epsilon$  turbulence model. In order to validate the CFD model, experiments involving an inclined solar chimney attached to a single room were performed. The experimental results agree reasonably well with the CFD calculations, with a 5.14% deviation between the values. Moreover, a Multi-Objective Genetic Algorithm (MOGA) coupled with Design of Experiments (DOEs) and the Response Surface Method (RSM) was employed to derive the optimal solar chimney design for the enhancement of indoor air motion. The optimization results reveal that the maximum indoor air speed in the living zone is achieved using a solar chimney of 1.85 m height, 2.65 m width, 75° inclination angle, and 0.28 m air gap. Sensitivity analyses indicate that solar chimney width is the most influential parameter, followed by inclination angle and then air gap, while the solar chimney height has a negligible effect. The proposed solar chimney is able to passively induce air motion of up to 0.28, 0.47, and 0.52 m/s at mean solar radiation values of 500, 700, and 850 W/m<sup>2</sup>, respectively. These elevated air velocities are capable of enhancing thermal comfort upper limits by removing sensible and latent heat from the body.

### 1. Introduction

Egypt's economy has grown dramatically in the 21st century after going through a deep recession in the late 1990s (Bolbol et al., 2005). This economic boom has resulted in swift growth in all development sectors including both the building and construction industries. Consequently, the country's primary energy consumption is rising alarmingly, having tripled in the last two decades (Egyptian Electricity Holding Company-Annual Report 2015/2016, n.d.) and experienced a 8.6% deficit between electricity generation and demand in 2013 (Dabaieh et al., 2015). With a population of ~90 million invariably driving the growth of housing project construction, the residential building sector consumes about 52% of the annual consumed energy (see Fig. 1), compared to 44.2% in 2014 (Attia et al., 2012). This percentage is expected to increase substantially due to increasing building-

sector investment and urban sprawl in newly developed cities.

Thermal comfort is a central concern in Egypt, which features a hot climate, considering that humans spend up to 80% of their time indoors, in a closed environment (O'Connor et al., 2016). Notwithstanding, sustainable construction features such as durability, passive solar design, and construction materials have not generally attained serious prominence to date (Ali Ahmed, 2012; Attia et al., 2013, 2012; Mahdy and Nikolopoulou, 2014; Saleem et al., 2016a; Saleem et al., 2014).

Generally speaking, most residential buildings are designed and built considering only economic and functional issues, without a comprehensive awareness of the environmental and energy consumption implications of such approaches; this approach arises primarily from (1) a lack of restrictive thermal specifications in the governmental building codes, and (2) a lack of awareness among local architects.

\* Corresponding author at: Energy Resources Engineering Department, Egypt-Japan University of Science and Technology, Alexandria, Egypt.  
E-mail addresses: [ahmed.saleem@ejust.edu.eg](mailto:ahmed.saleem@ejust.edu.eg), [aabdeen@aun.edu.eg](mailto:aabdeen@aun.edu.eg) (A. Abdeen).

<https://doi.org/10.1016/j.solener.2019.01.063>

Received 29 October 2018; Received in revised form 3 January 2019; Accepted 21 January 2019

Available online 24 January 2019

0038-092X/ © 2019 International Solar Energy Society. Published by Elsevier Ltd. All rights reserved.

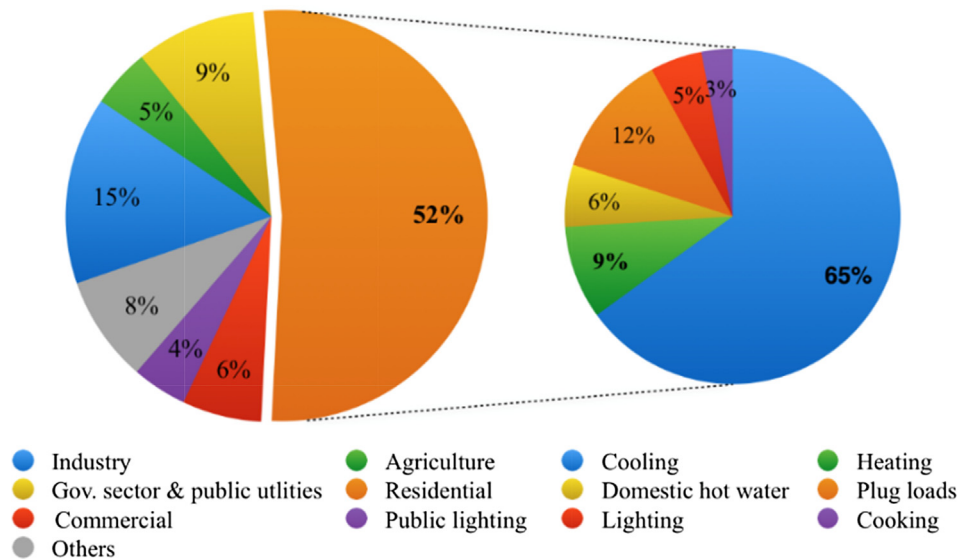


Fig. 1. Energy distribution profile in Egypt.

Consequently, reliance on mechanical devices to provide comfortable indoor environments for building occupants has been vastly increased, especially with government’s heavily subsidized domestic energy. Almost 65% of the total annual energy consumption in any residential building is attributed to cooling and ventilation (Ibrahim, 2011), as shown in Fig. 1.

In acknowledgment of this critical issue, the Egyptian government declared a reduction in subsidized domestic energy costs in 2014 and seeks to satisfy 20% of the electric energy demand from renewable energy resources by the year 2020 (Ibrahim, 2011). In this context, passive design approaches hold great promise for cooling buildings without resorting to mechanical appliances to provide adequately comfortable conditions. In hot climates, air movement is an essential contributor to perceived thermal comfort as it affects body heat transfer to the environment through convection and evaporation.

Previous studies of naturally ventilated buildings affirm that elevated air speeds can offset indoor temperature increases by removing sensible and latent heat from the body so that body temperatures are restored to a comfortable range (Ho et al., 2009; Nicol, 2004; Paliaga, 2009; Schiavon and Melikov, 2008; Yang and Zhang, 2009). According to the comfort-adaptive approach recently developed in ASHRAE (2010), the operative temperature comfort limits are based on a 0.2 m/s indoor air speed. However, elevated indoor air speeds are capable of augmenting these comfort limits. The relationship between air speed and operative temperature upper limit is depicted in Fig. 2. It has been

observed that the increase in operative temperature cannot be higher than 3.0 °C above the comfort-zone values, and that the elevated air speed must not be greater than 0.8 m/s.

Solar chimneys show promise for the enhancement of air movement in naturally ventilated buildings using renewable and clean sun energy. Air movement, in turn, enhances indoor comfort, which can drastically reduce energy consumption and related environmental effects due to year-round air conditioning. Egypt has abundant sunny and clear skies, with a daily average solar energy of 4.9 kWh/m<sup>2</sup> (Saleem et al., 2016b). These climatic features encourage the application of solar chimneys to provide comfortable conditions in residential buildings.

Indeed, the concept of incorporating solar chimneys into buildings is not new; solar chimneys have been investigated by numerous scholars due to their potential advantages in terms of energy requirements, economic impacts, and environmental benefits. A steady-state mathematical model was developed based on the thermal network approach to predict the induced natural ventilation using passive solar chimneys by Bansal et al. (1993). Similar approaches were also employed by Al-Kayiem et al. (2014), Ong (2003), Saleem et al. (2016c). Further, Hamdy and Fikry (1998) theoretically investigated the theoretical effect of different solar chimney tilt angles during summer in Egypt; they found that a 60° tilt angle is optimal in terms of the natural ventilation rate. Additionally, their findings demonstrate that increases in the air flow rate through a solar chimney are proportional to the stack height. Imran et al. (2015) also found a maximum ventilation rate at a 60° inclination angle using a chimney featuring a 5 cm gap and a 2 m height and width; the ventilation rate was ~20% higher at this inclination angle than at an angle of 45°. This study found a maximum air velocity of 0.8 m/s inside the gap for a solar intensity of 750 W/m<sup>2</sup>. Chen et al. (2003) experimentally investigated the thermal performance of solar chimneys with variable chimney-gap-to-height ratios and different inclination angles using a uniform heat flux; they showed that a solar chimney of 0.2 m channel depth, 1.5 m stack height, and 45° tilt angle can achieve a maximum flow rate 45% greater than that in a vertical chimney. Furthermore, Jing et al. (2015) built a solar chimney experimental set-up with large gap-to-height ratios between 0.2 and 0.6; the experimental results reveal that a gap-to-height ratio of 0.5 maximizes the air flow rate through the chimney. Furthermore, this study developed a new, improved model to predict the air flow rate, especially for chimneys with large gap-to-height ratios. Khanal and Lei (2014) studied the effect of absorber inclination angles ranging from 0° to 6° in an inclined passive wall solar chimney (IPWSC) with a uniform heat flux (100–500 W/m<sup>2</sup>) and a fixed channel depth of 0.1 m; they

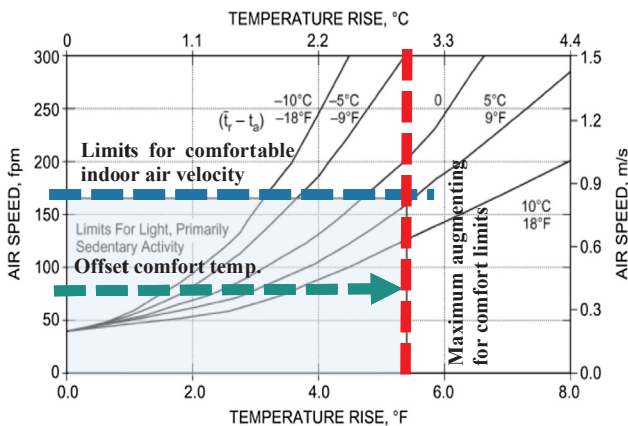


Fig. 2. Air speed required to offset the thermal comfort zone (ASHRAE, 2010).

revealed that a 6° tilt angle can induce the ventilation rate required by the ASHRAE standards. Different inclination angles for various air gaps were examined by (Siva Reddy et al., 2012); their measured experimental results indicate that the maximum ventilation rate of 0.32 m<sup>3</sup>/s occurs at a 50° inclination angle and a 10 cm air gap. Kumar et al. (1998) analyzed bioclimatic architecture assisted by a passive solar chimney for the promotion of natural ventilation and the reduction of indoor air contaminants in India.

Numerical CFD tests have also been widely used to examine buoyant air flow through solar chimneys. Harris and Helwig (2007) employed CFD analysis to scrutinize the effect of inclination angle, double glazing, and low-emissivity finish on solar chimney thermal performance. A solar chimney with a 67° tilt angle achieves 11% greater efficiency regarding flow rate than does a vertical chimney. Moreover, the use of a low-emissivity wall surface increases efficiency by 10%. Amori and Mohammed (2012) developed an unsteady, two-dimensional CFD model to predict the thermal performance and fluid flow patterns inside a solar chimney; their results agree fairly well with the experimental data.

Several groups have also employed three-dimensional models. Awbi and Gan (1992) modeled air movement and air flow rate inside a chimney using a CFD technique with a *K-ε* turbulence model; the predicted numerical results are quite consistent with the experimental results obtained by Bouchair (1994). Suárez-López et al. (2015) made a detailed numerical exergetic analysis of a solar chimney, showing a 1.4047 W difference between the inlet and exit flow exergies with a ventilation power of 0.0016 W; the thermal exergy efficiency was 0.55%, and the useful exergy efficiency was 0.0006%.

Recently, Tan and Wong (2013) developed a regression model to derive the optimum solar chimney design in tropical conditions; they then extended this work (Tan and Wong, 2014) by investigating the effect of ambient air speed and internal heat load on solar chimney thermal behavior using a CFD technique. Similar methodology has been employed in different solar chimney power plants by Kasaeian et al. (2014), Patel et al. (2014).

Attempts have also been made to enhance indoor thermal comfort using passive solar chimneys. For example, Khedari et al. (2000b) conducted experiments on the effects of air gap on the induced air flow rate and thermal comfort in a roof-top solar chimney (RTSC). In that study, two RTSC units of 1.5 m<sup>2</sup> each were integrated into the south-facing roof of a 30 m<sup>3</sup> single room; the observations reveal an average air change rate (ACH) of ~4–5, which is not sufficient to satisfy comfort guidelines. Khedari et al. (2000a) extended their work by experimentally investigating various solar chimney configurations in a single-room school house of 25 m<sup>3</sup> to increase air speed within the space. Three different solar chimney configurations were integrated into the southern wall, while two RTSC configurations were installed on the southern roof. The resulting ACH values varied between 10 and 15; however, the induced air motion at the living level was about 0.04 m/s, which does not satisfy the thermal comfort requirements for occupants. Though growing interest has been devoted to optimizing solar chimney performance, most endeavors deal primarily with enhancing ventilation rates for improved indoor air quality; investigations of enhanced thermal comfort through increasing induced air stream within the space are relatively rare. Additionally, these studies are unable to consider the cumulative impact of variation in all parameters, which may produce a different optimum design.

This research gap spurred both our investigation of the efficiency of using an inclined solar chimney to elevate indoor air motion and our particular emphasis on occupant comfort. In the present study, a Multi-Objective Genetic Algorithm (MOGA) coupled with Design of Experiments (DOEs) and a Response Surface Method (RSM) using an ANSYS®17.2 package was employed to derive an optimal solar chimney design for the improvement of indoor air motion and thermal comfort. Such optimization methods can integrate all chimney parameters: height, width, inclination angle, and the air gap between the glass and

absorber wall. This methodology was validated against an experimental investigation of an inclined solar chimney attached to a single room. Finally, CFD experiments were performed to predict the detailed space flow patterns and velocity fields in the optimal design under different solar intensities.

## 2. Experimental configuration

A cubic wooden room with an area of 4 m<sup>2</sup> and internal volume of 8 m<sup>3</sup> was constructed in the city of Alexandria, Egypt at a longitude and latitude of 31.2°N and 29.91°E, respectively. The solar chimney was installed on the roof of this room and oriented south to draw fresh air from a 0.6 m × 0.6 m north-facing window with a window-to-wall ratio of 16%. This chimney consisted of an absorber wall measuring 1.4 m in height and 0.6 m in width and made of a 1 mm ductile steel sheet glued and painted matte black. The south side of the chimney was covered by standard 4 mm float glass with a 0.25 m air channel gap and without an emissivity coating that would make the glass opaque to infrared radiation. In this study, heat loss from the back and sides is nearly eliminated through the use of 0.05 m-thick glass wool insulation around the absorber.

Six T-type thermocouples with an accuracy of up to ± 0.3 °C were used for temperature measurements at different points in the chimney as detailed in Fig. 3; thermocouples were fixed on the midline of the absorber surface, the inner surface of the glass, and the air flow region. Similarly, two WE300 solar radiation pyranometers with an accuracy of 1% were connected to the test setup; the first one was placed on the top of the outer glass face to measure the ambient solar intensity, and the other was placed on the absorber surface to measure the radiation flux on the absorber surface. Both pyranometers were inclined at the same angle as the solar chimney. Air velocity was measured at the center of the chimney inlet using a sensitive hot-bead anemometer (TSI 9545 VelociCalc Hot Wire Anemometer) with a maximum error of ± 0.015 m/s. Data for all of these instruments were recorded every 15 min from 10:00 to 16:00 using a multipoint digital data logger (remote scanner NEC DC 6100). A schematic of the temperature, air velocity, and solar radiation instruments can be found in Fig. 3. Weather data such as ambient dry bulb temperature, solar intensity, and wind speed were recorded simultaneously using a PortLog weather station installed close to the experimental measurement site.

## 3. Numerical modeling

Fig. 4 depicts the physical setting of the solar chimney, which is directly attached to a ventilated space. In the present study, the ANSYS®17.2 Fluent commercial CFD software program was employed to develop a three-dimensional numerical model. The experimental geometry was recreated exactly in the ANSYS DesignModeler program.

### 3.1. CFD governing equations

The basic assumptions for the CFD simulations included three-dimensional, fully turbulent, and incompressible flow. The governing equations were solved on a staggered grid using the Finite Volume Method (FVM). The Semi-Implicit Method for Pressure-Linked Equations (SIMPLE) algorithm was applied to couple the continuity and momentum equations through pressure. For gradient and pressure discretization, a least-squares, cell-based pressure staggering option (PRESTO!) method was applied; momentum, energy, turbulence kinetic energy dissipation rate, and discrete ordinates were discretized using second-order upwind methods. All thermo-physical fluid properties are assumed to be invariant except for density in the buoyancy force term; this density term can be adequately modeled by the Boussinesq approximation, which delivers faster convergence than models with fluid densities that vary as a function of temperature (Ansys Fluent, 2015). Thus, the governing equations can be written as follows:

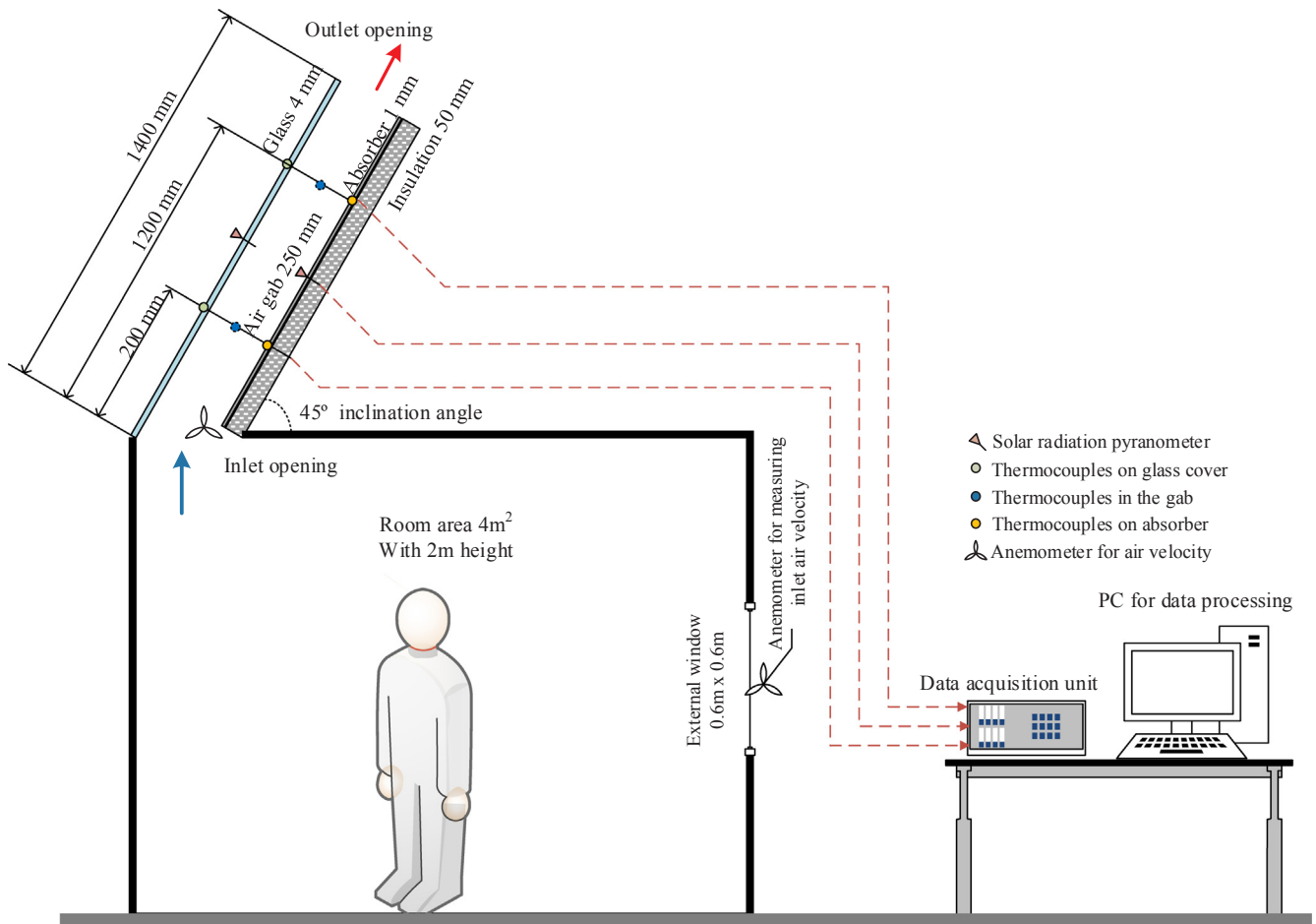


Fig. 3. Measurement instrument configuration in the experimental set-up.

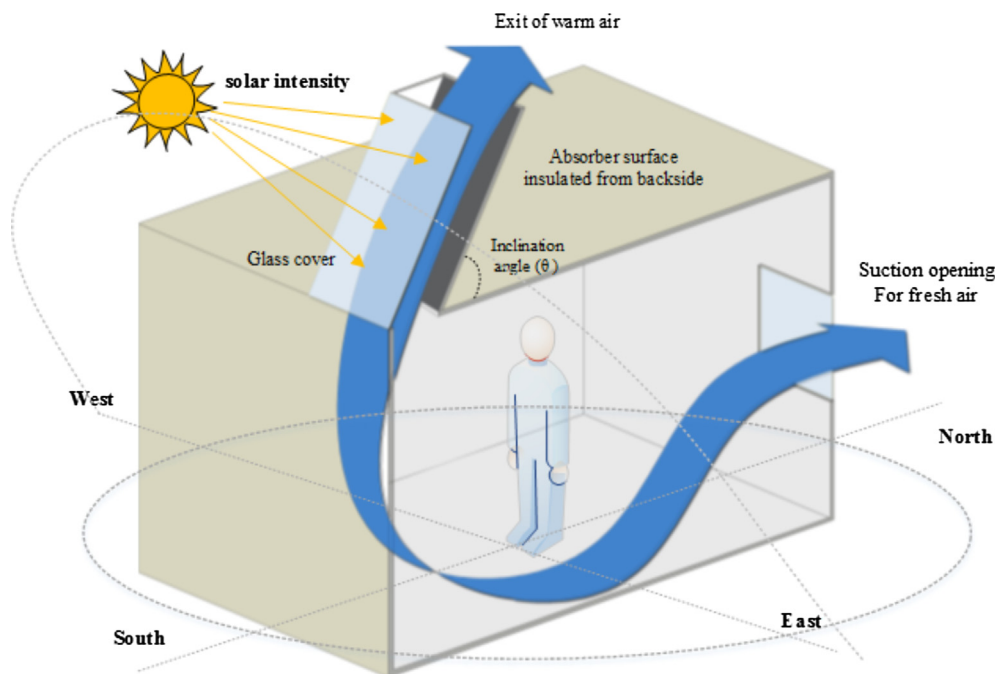


Fig. 4. Ventilation flow diagram of a single room with a solar chimney.

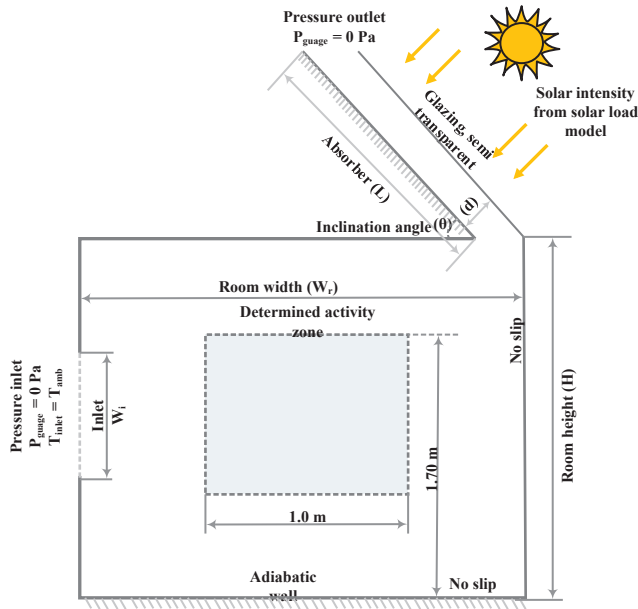


Fig. 5. Schematic of the computational domain with boundary conditions.

$$\nabla \cdot (\rho \vec{v}) = 0 \tag{1}$$

$$\rho \vec{v} + \nabla \vec{v} = -\vec{\nabla} P + \vec{\nabla} \cdot \dot{\tau} + \rho \vec{g} \tag{2}$$

$$\rho c_p \vec{v} \cdot \nabla T = \kappa \nabla^2 T + \vec{\nabla} \cdot \dot{\tau} \vec{v} \tag{3}$$

where  $\rho$  is density,  $\vec{v}$  is fluid velocity,  $\nabla = \frac{\partial}{\partial x} + \frac{\partial}{\partial y} + \frac{\partial}{\partial z}$ , and  $\dot{\tau}$  is the Reynolds stress tensor, which represents the effect of turbulent velocity fluctuations on fluid flow.

Eqs. (1)–(3) are the continuity, momentum, and energy equations, respectively. As shown, the governing equations do not include the transient term because all of the simulations were performed at specific times (i.e., hourly from 10:00 to 16:00). To ensure numerical stability, the absolute convergence was considered to be achieved when the sum of the normalized residuals for the discretized equations was less than  $10^{-4}$ .

### 3.2. Turbulence modeling

Various turbulence models have been used in the literature to model natural convective flow problems. Among them, the standard  $k-\epsilon$  model, the Reynolds Stress model (RSM), and the renormalization group (RNG)  $k-\epsilon$  model are commonly used to model natural convective flow within different solar chimney configurations (Gan, 2006; Gan and Riffat, 1998; Khanal and Lei, 2015; Serageldin et al., 2016; Sudprasert et al., 2016). In this study, the RNG  $k-\epsilon$  turbulence model was applied to model air turbulence as described in a study by Chen (1995), which examined indoor air flow under different turbulence models and concluded that the RNG  $k-\epsilon$  model was the most accurate model in terms of flow separation, streamline curvature, and flow stagnation.

The RNG  $k-\epsilon$  turbulence model is a semi-empirical model based on the transport equations for the turbulence kinetic energy ( $k$ ) and its dissipation rate ( $\epsilon$ ) that was derived using an accurate statistical method (i.e., not by experimentation). This model can be employed to near-wall regions without the addition of wall functions in the transport equations (Calautit et al., 2013). The main difference between the standard and RNG  $k-\epsilon$  turbulence models is the additional term in the  $\epsilon$  equations, which significantly improves the accuracy of turbulent flows. In the derivation of the RNG  $k-\epsilon$  model, the flow is considered fully turbulent and molecular viscosity effects are neglected. The turbulence kinetic energy ( $k$ ) and rate of dissipation ( $\epsilon$ ) are obtained from

Table 1  
Thermo-physical properties of materials.

Properties	Air	Glass	Steel	Wood	Insulation
Density (kg/m <sup>3</sup> )	Boussinesq = 1.18	2220	8030	700	10
C <sub>p</sub> (Specific Heat) (J/(kg K))	1006.43	830	502.48	2310	830
Thermal Conductivity (W/(m K))	0.0242	1.15	16.27	0.173	0.1
Viscosity (kg/(m s))	1.7894E-5	-	-	-	-
Thermal Expansion Coefficient (1/K)	0.00335	-	-	-	-

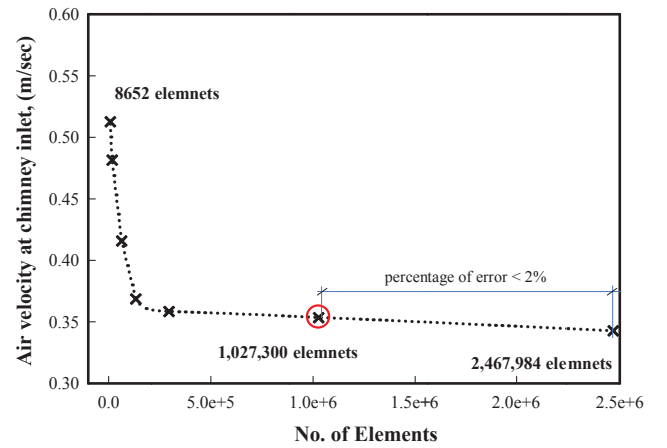


Fig. 6. Air velocity versus number of grid elements.

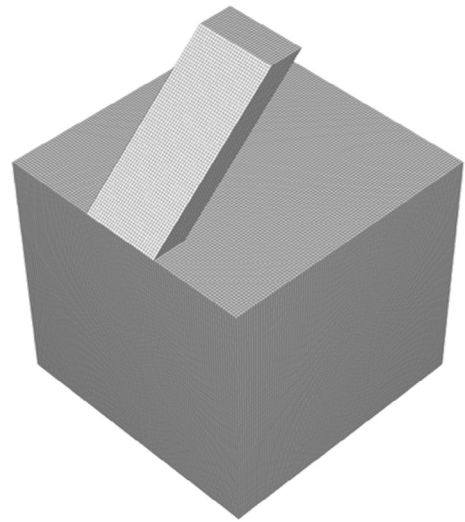


Fig. 7. Hexahedral mesh structure used for CFD simulations.

the following transport equations:

$$\nabla \cdot \rho k \vec{v} = \nabla \cdot \left( \mu + \frac{\mu_t}{\sigma_k} \right) \nabla k + G + B - \rho \epsilon_k \tag{4}$$

$$\nabla \cdot \rho \epsilon \vec{v} = \nabla \cdot \left( \mu + \frac{\mu_t}{\sigma_\epsilon} \right) \nabla \epsilon + C_{1\epsilon} \frac{\epsilon}{k} G + C_{1\epsilon} (1 - C_{3\epsilon}) B - \left( C_{2\epsilon} \rho + \frac{C_\mu \eta^3 (1 - \eta/\eta_0)}{1 + \beta \eta^3} \right) \frac{\epsilon^2}{k} \tag{5}$$

In Eqs. (4) and (5),  $C_{1\epsilon}$ ,  $C_{2\epsilon}$ , and  $C_{3\epsilon}$  are constants with empirical values of 1.45, 1.82, and 0.09, respectively (Khanal and Lei, 2015).  $\sigma_k$  and  $\sigma_\epsilon$  are the turbulent Prandtl numbers for  $k$  and  $\epsilon$  and have empirical values of 0.8 and 1.15, respectively (Khanal and Lei, 2015).  $G$

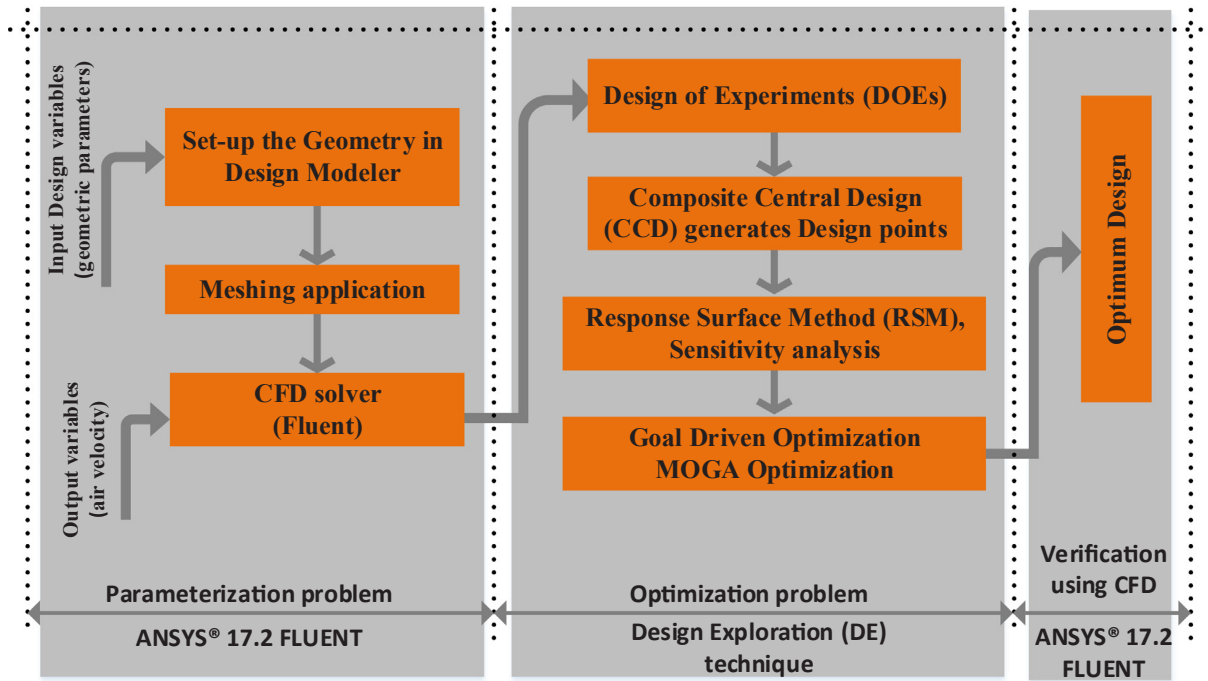


Fig. 8. Flow chart of the design exploration algorithm.

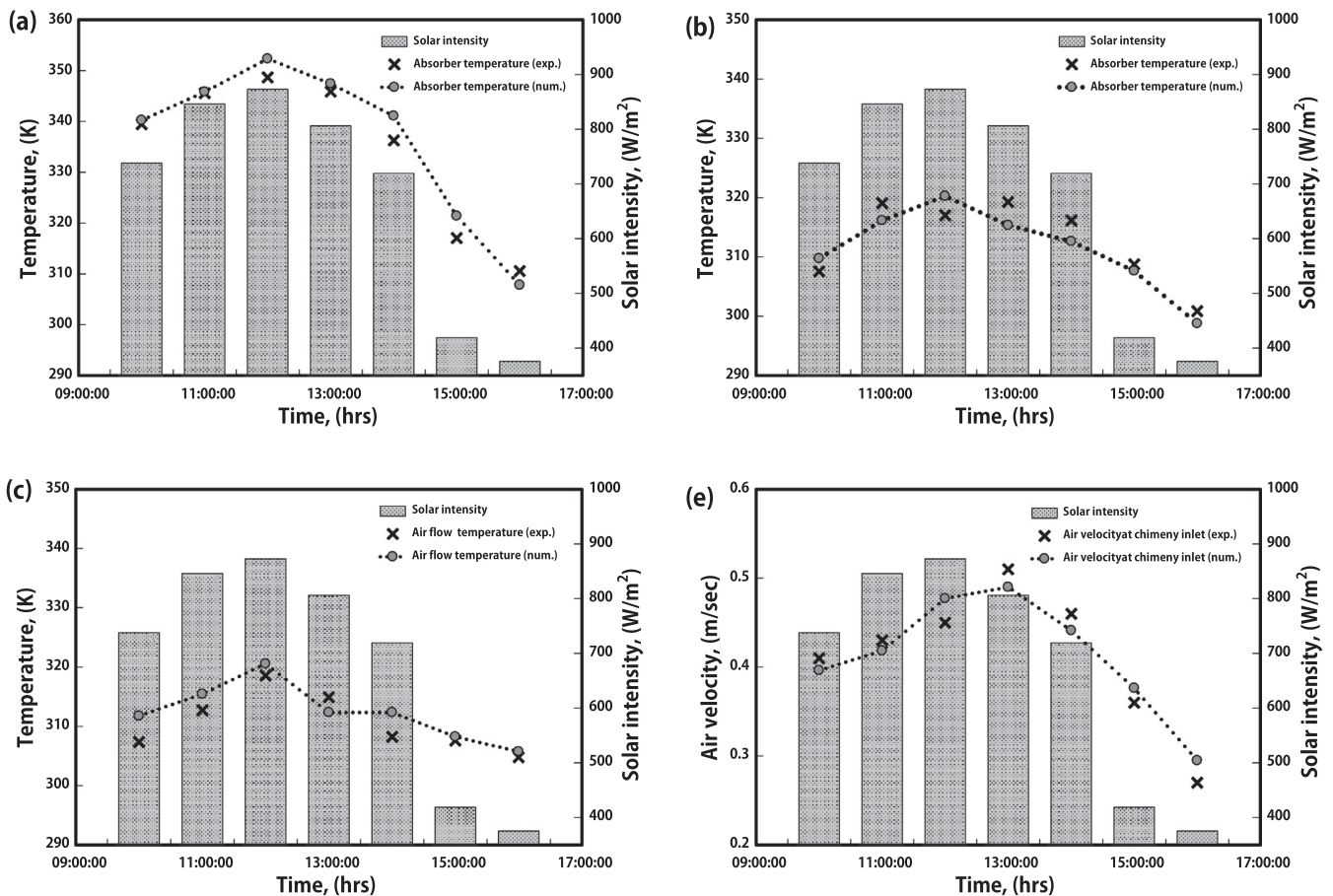


Fig. 9. Comparison between numerical and experimental results for the (a) absorber surface temperature, (b) glass temperature, (c) air flow temperature, and (e) air velocity at chimney inlet.

**Table 2**  
Design points generated from the Design of Experiments (DOEs).

Design points	air gap (m)	Chimney width (m)	Inclination angle (°)	Stack height (m)
1	0.2	2.75	28	1.92
2	0.288	2.65	46	2.04
3	0.192	0.85	68	1.76
4	0.208	2.95	56	1.8
5	0.128	1.55	42	2.4
6	0.216	1.75	26	2.32
7	0.248	2.55	72	2.2
8	0.28	1.15	54	1.68
9	0.296	1.35	40	2.24
10	0.168	1.95	74	2
11	0.136	1.65	34	1.56
12	0.24	2.35	48	2.48
13	0.232	1.05	32	1.84
14	0.272	1.25	70	2.16
15	0.16	2.85	52	2.36
16	0.104	2.45	60	1.88
17	0.256	2.05	36	1.6
18	0.264	2.15	66	1.64
19	0.144	0.65	44	1.72
20	0.12	2.25	38	1.96
21	0.112	0.95	62	2.08
22	0.176	1.85	58	1.52
23	0.184	1.45	64	2.44
24	0.152	0.75	30	2.12
25	0.224	0.55	50	2.28

modeled on all heated surfaces. The absorber plate was considered adiabatic from the backside, where 5 cm of insulation was provided to prevent direct heat transfer from the chimney to the ambient environment (Fig. 5). The thermo-physical properties of the solid and fluid materials used in this simulation are depicted in Table 1.

The ambient conditions at the outermost boundaries were represented using temperature and inlet velocity values from field measurements and assuming a pressure of 1 atm. Further, the acceleration of gravity was considered; its value was set equal to 9.81 m/s<sup>2</sup>.

A solar load model was used to model the direction and irradiance of the direct normal solar beam entering the computational domain. The solar load model included a solar calculator with the option to control the sun’s location for a given time of day, date, and position (Ansys Fluent.co, 2015). In this model, the solar ray tracing algorithm computed the heat flux on the boundary faces using the direction and magnitude of the incident solar radiation. A pressure inlet with zero-gauge pressure boundary condition was prescribed for the room inlet. The incoming air was assumed to be at the measured ambient temperature. At the chimney exit, a pressure outlet boundary condition was prescribed in which the fluid pressure was assumed to be equal to the ambient pressure and the stream-wise variations in the velocity components, temperature, turbulent kinetic energy, and dissipation rate were assumed to be negligible.

3.4. Grid resolution test

The accuracy of the numerical results was ascertained by a grid independence study, which was performed on seven mesh densities with hexahedral cells ranging from 8652 to 2,467,984 elements as depicted in Fig. 6. Air velocity, the parameter of interest, can quantify the effectiveness of the solar chimney in terms of thermal comfort and was thus chosen for comparison. Simulations were performed on a structured, non-uniform mesh created with hexahedral elements (see Fig. 6); a coarser mesh was used, as it can provide sufficient spatial resolution at computational times much lower than those required by a finer mesh. The applied boundary conditions remained fixed throughout the simulation process to ascertain precise comparisons. The inlet air velocity stabilized at ~0.353 m/s at 1,027,300 elements. Fig. 6 shows that the percentage of error between the grid refinements was minimized (at < 2%) for the benchmark model at 1,027,300 elements (see Fig. 7).

4. Design optimization

It is worth mentioning that, in the literature (please refer to Section 1), improvements in solar chimney performance depend significantly on the design variables. Relevant design variables include geometric parameters that control the shape of the solar chimney, such as height, width, inclination angle, and channel spacing. To optimize solar chimney performance and provide detailed and accurate results, almost all of the parameter probabilities must be scrutinized, which requires an enormous number of CFD simulations. This study employed the ANSYS®17.2 FLUENT Design Exploration (DE) technique to optimize the solar chimney geometry, placing particular emphasis on induced air motion for the enhancement of indoor occupant comfort; Design Exploration (DE) is an optimization module that derives the optimal design variables based on the design constraints and objective function. In this method, several criteria (such as ‘maximize,’ ‘minimize,’ or ‘determine target value’) are used to explore chimney performance through one or more output parameters.

The overall optimization process encompasses the initial sampling step through Design of Experiments (DOEs), followed by the appropriate interpolation technique using a Response Surface Method (RSM); finally, the data from the preceding two steps are used for optimization in a Multi-Objective Genetic Algorithm (MOGA). The detailed optimization procedures are depicted as a flowchart in Fig. 8. Initially, the

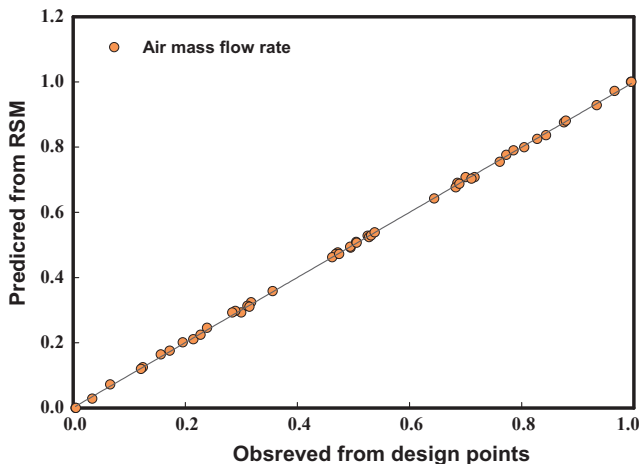


Fig. 10. A Goodness of Fit (GoF) chart showing output parameter values simulated by CFD versus those predicted from RSM.

represents the generation of turbulent kinetic energy due to the mean velocity gradient and *B* is the generation of turbulence kinetic energy due to buoyancy; these variables can be expressed as:

$$G = -\rho u'_i u'_j \frac{\partial u_i}{\partial x_j} \text{ and } B = g_i \beta \frac{\mu_t}{Pr_i} \frac{\partial T}{\partial x_i} \tag{6}$$

In the  $\epsilon$  equation (Eq. (5)),  $\eta$  is defined as:

$$\eta = S \frac{k}{\epsilon} \text{ where } S = \sqrt{\frac{G}{\mu_t}} \tag{7}$$

3.3. Boundary conditions

The air flow and temperature response within the represented computational domain were modeled under quasi-steady-state conditions; standard wall functions were used for the turbulence model, and a rigid no-slip condition was prescribed on all vertical and horizontal walls. Conductive, convective, and radiative heat transfer were

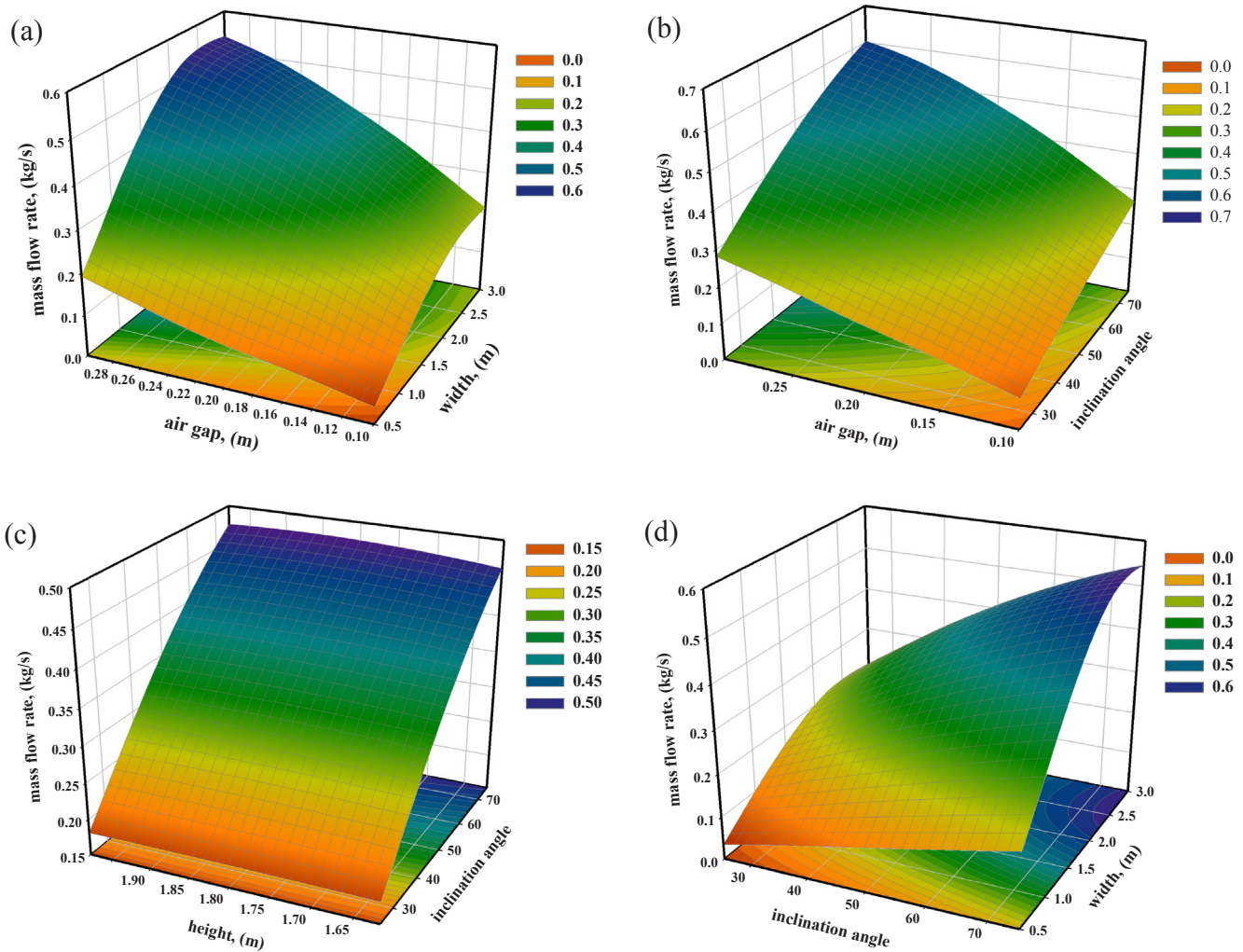


Fig. 11. Response surfaces of mass flow rate versus solar chimney parameters: (a) width and air gap, (b) inclination and air gap, (c) height and inclination angle, and (d) width and inclination angle.

solar chimney design variables (height, width, air gap, and inclination angle) were defined in the Design Modeler. The mass flow rate and average air velocity in the activity zone were introduced as an output parameter in the fluent solver. The complete analysis of the initial design included drawing, meshing, solving the governing equations, and defining inputs and parameters.

4.1. Design of experiments (DOEs)

The large number of tests required to obtain the optimal solar chimney design are quite time-consuming and not efficient from an economic point of view. Moreover, traditional one-by-one experimental parameter optimization is implicit, and one could argue that the cumulative impact of all parameters might produce a different optimal design. A DOEs approach was taken to the CFD simulations to provide an explicit conclusion. DOEs is a branch of statistics that explores interactions between design and output variables through a minimum number of sampling points; this technique randomly distributes the experiments throughout the design space based on the fit of a multi-factor linear regression model to the data. In this study, a minimum-density design point grid spanning the multivariable design space was generated using the Optimal Space Filling Design (OSFD) technique, which was selected for its ability to provide large amounts of information with a minimum number of numerical simulations; OSFD is an extension of Latin Hypercube Sampling Design (LHS) that involves

post-processing (Ansys Fluent.co, 2015).

4.2. Response surface method (RSM)

The Response Surface Method (RSM), which is used extensively to optimize industrial applications, is an explicit approximation function that produces correlations between input and output parameters used by the fitting algorithm indicated in the DOEs methodology. The RSM is obtained using the second-order polynomial regression model set and the results generated from the DOEs, which can be written as follow (Al Jubori et al., 2017):

$$f = \beta_0 + \sum_{j=1}^n \beta_j x_j + \sum_{j=1}^n \beta_{jj} x_j^2 + \sum_{i=1}^n \sum_{j=1, i \neq j}^n \beta_{ij} x_i x_j \tag{8}$$

These correlations reflect the relationships between the design parameters and the response surface, where  $f$  is the response,  $x$  is the design variable,  $n$  is the number of design variables, and  $\beta_0, \beta_1$ , etc. are regression coefficients.

4.3. Goal driven optimization

The Design Exploration module in ANSYS®17.2 FLUENT applies a distinctive approach in which the Pareto optimal solution is used for the multi-objective optimization; this involves a set of optimal solutions that are inconsistent with each other (Ansys Fluent.co, 2015). After the

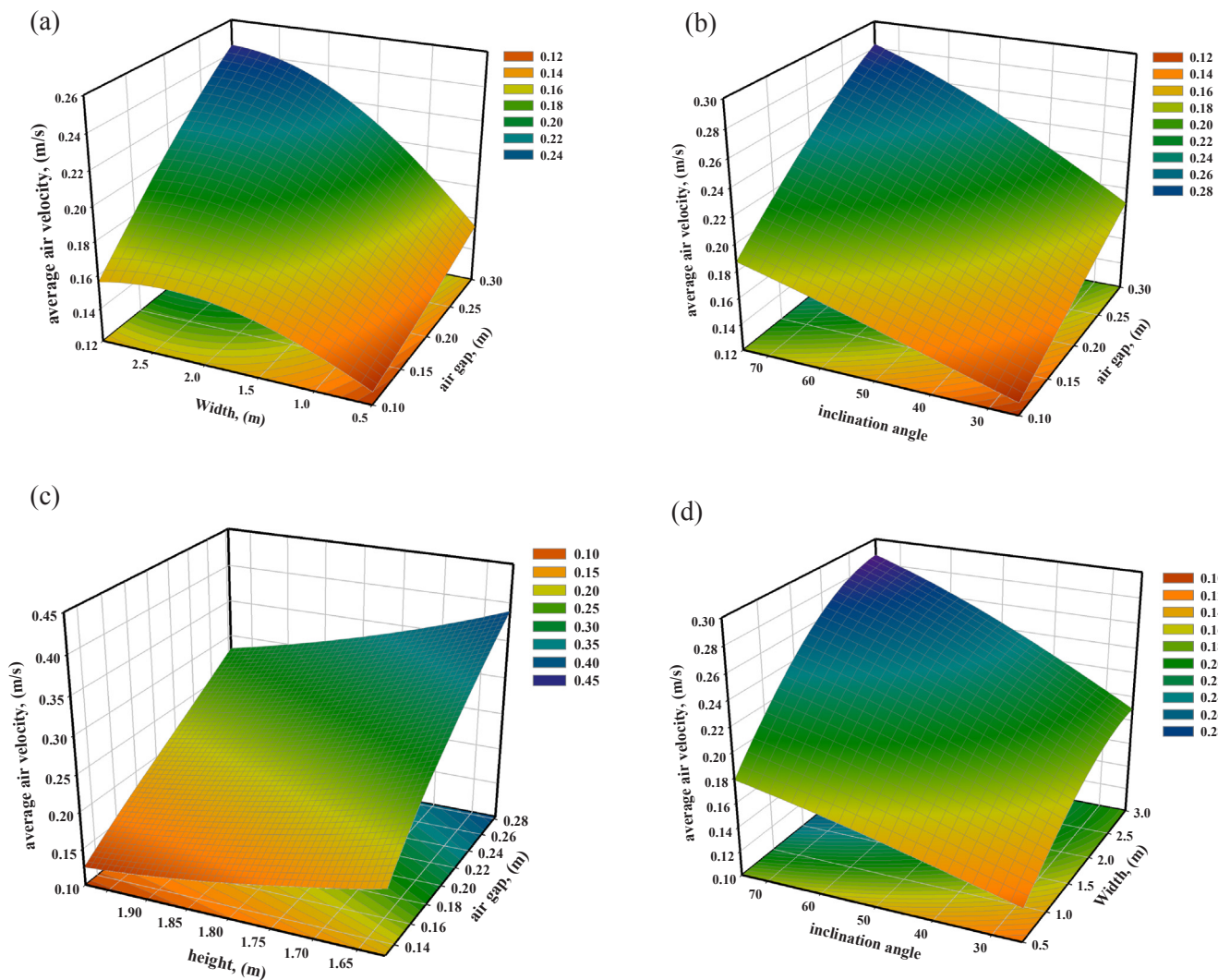


Fig. 12. Response surfaces of average velocity in the activity zone versus solar chimney parameters: (a) width and air gap, (b) inclination and air gap, (c) height and air gap, and (d) width and inclination angle.

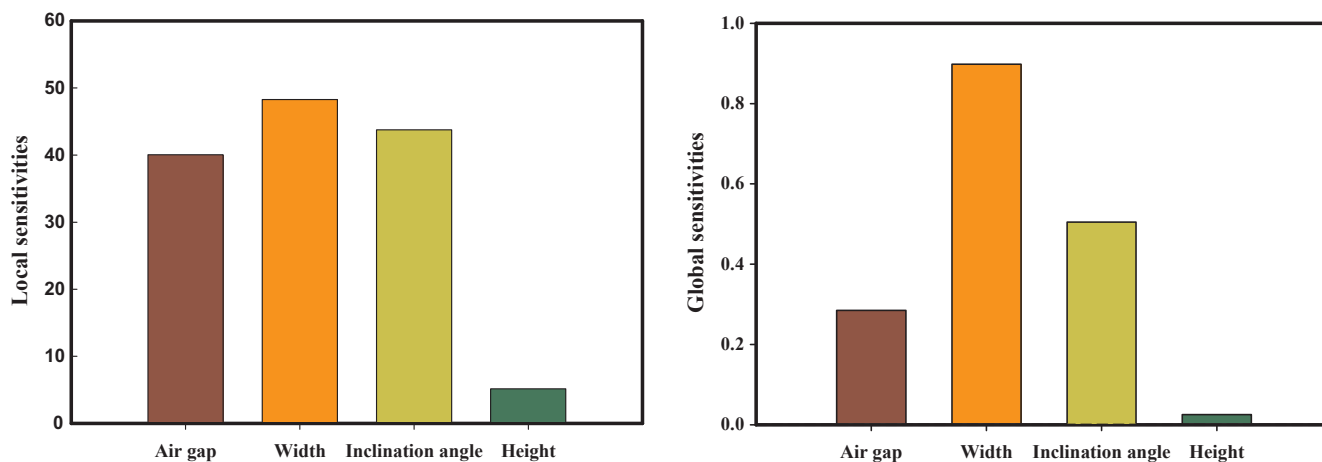


Fig. 13. Global (right) and local (left) sensitivities of solar chimney design variables.

response surface data has been produced, so-called Goal Driven Optimization (GDO) is performed. In this study, the MOGA algorithm was applied to derive the optimal design based on the targets sets by maximizing the mass flow rate and average velocity in the activity zone. MOGA is an evolutionary algorithm with several objective

functions that are optimized simultaneously and subject to inequality and equality constraints (Ansys Fluent.co, 2015). This algorithm can be expressed mathematically in vector form as (Ennil et al., 2016):

The objective function vector:

**Table 3**  
Design parameter ranges.

Design parameter	Minimum value	Maximum value
Air gap (m)	0.1	0.3
Solar chimney width (m)	0.5	3.0
Inclination angle (°)	25	75
Solar chimney height (m)	1.5	2.5

**Table 4**  
Three optimal chimney design candidates with regard to the desired objectives.

	Candidate #1	Candidate #2	Candidate #3
Air gap (m)	0.28	0.28	0.28
SC width (m)	2.65	2.73	2.68
Inclination angle (°)	75	74.6	74.15
SC height (m)	1.85	1.85	1.85
Mass flow rate (kg/s)	0.6848	0.6834	0.6812
Average air velocity in activity zone (m/s)	0.3846	0.38412	0.3838

$$F(x) = [f_1(x), f_2(x), \dots, f_k(x)]^n \tag{9}$$

$$\text{Subject to: } g_i(x) \leq 0 \quad i = \{1, \dots, m\}$$

$$h_j(x) = 0 \quad j = \{1, \dots, p\}$$

where  $k$  is the dimensional space of the objective functions and  $g_i(x)$  and  $h_j(x)$  are the inequality and equality constraints, respectively.

## 5. Results and discussion

### 5.1. Experimental and validation results

To test the reliability and accuracy of the CFD model for inclined solar chimney calculations, the RNG  $k-\epsilon$  turbulence model simulation results are compared with the experimental measurements. Fig. 9 compares the numerically predicted and experimentally measured absorber temperature, glass temperature, air flow temperature, and air velocity at the chimney inlet under the same operating conditions. Reasonable agreement is achieved between the numerical predictions and experimental measurements, which highlights the ability of the 3D CFD model to accurately predict buoyancy-driven ventilation. The deviation between the numerical and experimental results ranges between 0.33% and 8.52% with an average of 5.14%, which can be compared to average errors of 14% and 23% in Imran et al. (2015), Mathur et al. (2006), respectively.

These error improvements may be attributed to heat loss from the chimney glass and room walls to the surroundings, which can be expressed using the following equation, as reported by Ong (2003):

$$h_{wind} = 5.7 + 3.8V \tag{10}$$

In both the experimental and numerical results, significant temperature differences in the chimney components are observed to correspond with the solar intensity; temperature increases linearly in all chimney components as the solar intensity increases. The glass surface temperature reaches a maximum of 335 K at a solar intensity of 850 W/m<sup>2</sup>. The temperature of air trapped within the chimney cavity is always higher than that of the glass surface due to convection from both sides and the very high temperature for the black absorber wall, which reaches 350 K at a solar intensity of 850 W/m<sup>2</sup>. The absorber surface is at higher temperature than both the glass and air flow due to additional captured radiation and the storage of a large amount of thermal energy. The energy absorbed by the black wall increases the air flow at the chimney inlet by about 0.5 m/s at a solar intensity of 850 W/m<sup>2</sup>.

### 5.2. Optimization results

Following the validation of the CFD model as discussed in Section 5.1, an extended 3D numerical model was developed with a square area 9 m<sup>2</sup> and a height of 3 m, which represents a typical room in an Egyptian dwelling. In this model, the applied boundary conditions were similar to those defined in Section 3.3, except for the inlet flow to the room, which was defined to pressure inlet. To obtain the optimal solar chimney geometry and design variables, CFD analysis coupled with MOGA optimization was performed at average summer operational conditions (solar intensity = 700 W/m<sup>2</sup>; ambient temperature = 305 K).

In the DOEs stage, a set of 25 design points were generated as shown in Table 2 using the OSFD technique and varied continuously over specified ranges. These ranges were selected to be consistent with Egyptian building laws and regulations. Initially, the generated design points were solved via new volume finite analyses in the Fluent solver in order to calculate the output parameters. In the current study, the genetic aggregation meta-model technique was chosen to generate response surface data. Using a sample set generated from the DOEs approach, a Goodness-of-Fit (GoF) chart was generated in order to examine the interpolation approach used for solar chimney optimization; the GoF graph shows the output parameter (mass flow rate) predicted from the response surface versus the values calculated from CFD simulations. It is evident from Fig. 10 that the interpolation approach used herein produces reasonably accurate predictions, as a smaller spread of points around a straight line indicates better predictions (Thompson et al., 2017).

Subsequently, the results generated by DOEs were fed to the RSM to examine the influence of solar chimney parameters on the mass flow rate and average velocity in the activity zone, as shown in Figs. 11 and 12, respectively. These figures demonstrate that both response variables increase almost linearly with increments in the solar chimney width, air gap, and inclination angle. However, no significant changes are observed with changes in chimney height. Consequently, the mass flow rate can be used as an indicator for average air velocity, which drives thermal comfort.

Fig. 13 highlights the local and global sensitivities of mass flow rate with respect to solar chimney parameters. Local sensitivity is defined as the sensitivity of the objective output to changes in one input parameter holding all other input parameters fixed, while global sensitivity evaluates the effects on the objective output of all of the changing input parameters acting simultaneously over their ranges of uncertainty (Haaker and Verheijen, 2004). Solar chimney width is the most sensitive parameter, followed by inclination angle, and then air gap, while the solar chimney height has a negligible effect. During global sensitivity analysis, all possible values of the input parameters are examined to determine these sensitivity values.

The MOGA method was applied to explore the optimal solar chimney design variables in relation to the objective function. The MOGA relies on the Non-Dominated Sorted Genetic Algorithm-II (NSGA-II), which is one of the most robust algorithms for solving multi-objective optimization problems; this strategy implements a “Pareto-optimal” solution to generate 10,000 designs in a single optimization run and sorts the samples according to the set objective, which in this case is the maximization of the mass flow rate and average velocity in the activity zone. Table 3 shows the three optimal designs according to the desired objectives and specified boundaries; these optimal designs feature a few slight differences (see Table 4).

### 5.3. CFD for comfort analysis

Candidate #1 (1.85 m height, 2.65 m width, 75° inclination angle, and 0.28 m air gap) is the optimal solar chimney design as it maximizes both mass flow rate and air velocity in the activity zone, which measure 0.6848 kg/s and 0.38 m/s, respectively. To examine the performance of

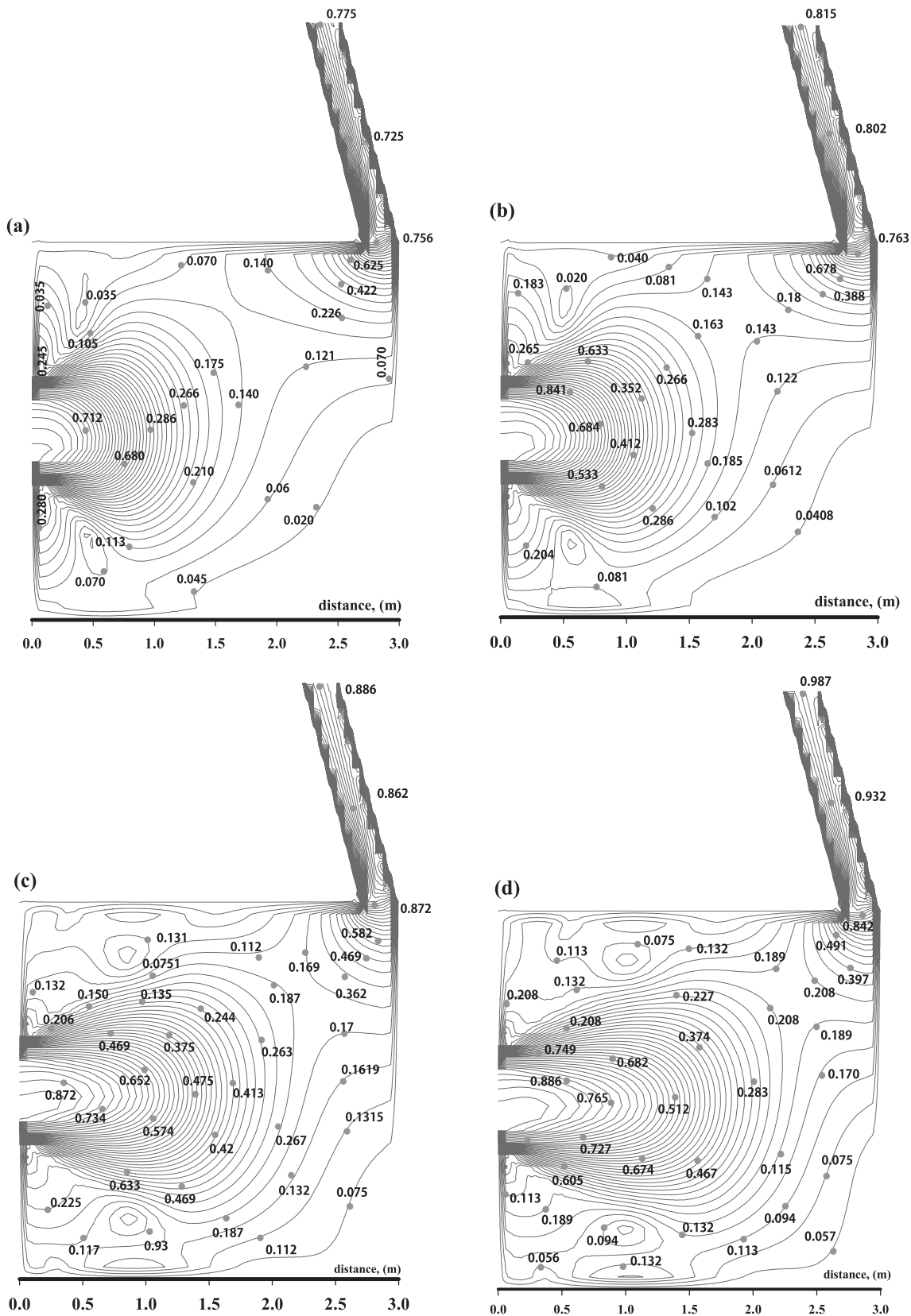


Fig. 14. Velocity contours resulting in the optimal solar chimney design at solar intensities of (a) 200, (b) 500, (c) 750, and (d) 850 W/m<sup>2</sup>.

the proposed solar chimney design in terms of comfort conditions, the optimal design was simulated under different solar intensity values. Fig. 14 shows contour plots of velocity for the considered geometry under different boundary conditions. It is clear that the

greatest velocity values generally appear at the window and chimney inlets and fill a significant portion of the space; however, flow is approximately stagnant in the corners of the room. Under the selected optimal design, it is interesting to note that there is no reverse flow

within the chimney under the different conditions examined; this can be explained by the narrow chimney inlet cross-section, which decreases the chance of fluid flow separation.

Under 700 and 850 W/m<sup>2</sup> of solar radiation, the indoor air velocity in the activity zone reaches 0.47 and 0.52 m/s, respectively. According to (ASHRAE, 2010), these air velocities offset the comfortable operative temperature by approximately 1.7 °C by removing sensible and latent heat from the body. At 500 W/m<sup>2</sup> of solar radiation, the induced air motion in the activity zone reaches 0.28 m/s, which can offset the comfortable operative temperature by ~0.9 °C. Solar radiation is considered to be the main force driving the solar chimney mechanism. Hence, at a low solar radiation of 250 W/m<sup>2</sup>, the induced buoyant air motion reaches only 0.14 m/s in the activity zone, which does not have a significant effect on the operative temperature.

## 6. Conclusions

In this paper, a three-dimensional quasi-steady CFD model was developed and validated against experimental results. Moreover, a novel optimization technique (using the ANSYS®17.2 FLUENT Design Exploration module) was used to ameliorate indoor occupant comfort by increasing the air velocity resulting from buoyancy effects inside the space. This optimization method can integrate a variety of chimney parameters, including the height, width, inclination angle, and air gap between the glass and the absorbing wall. Moreover, CFD simulations were performed to simulate the proposed optimal chimney design under different solar intensities and predict detailed flow patterns in the test space. The main achievements of this study can be described as follows:

- Results from the CFD model developed herein show reasonable agreement with the experimental results (5.14% average deviation).
- The optimal solar chimney derived from the optimization method, which features a 1.85 m height, 2.65 m width, 75° inclination angle, and 0.28 m air gap, successfully enhances thermal comfort under solar intensities higher than 500 W/m<sup>2</sup>.
- In terms of air motion induced by buoyant force, solar chimney width is the most sensitive parameter, followed by inclination angle, and then air gap. The effect of solar chimney height is negligible.

These findings clearly highlight the potential and advantages of employing this 3D optimization technique to enhance thermal comfort in Egyptian residential buildings by elevating indoor air velocity through the use of passive solar chimneys.

## Acknowledgments

The first author would like to thank the Egyptian Ministry of Higher Education for financial support (a Ph.D. scholarship), as well as the Egypt-Japan University of Science and Technology (E-JUST) for offering the facilities and tools needed to conduct this work. Furthermore, this research would not have been possible without the ongoing support of the Tokyo Institute of Technology in terms of tools and facilities.

## References

Al Jubori, A., Al-Dadah, R.K., Mahmoud, S., Bahr Ennil, A.S., Rahbar, K., 2017. Three dimensional optimization of small-scale axial turbine for low temperature heat source driven organic Rankine cycle. *Energy Convers. Manag.* 133, 411–426. <https://doi.org/10.1016/j.enconman.2016.10.060>.

Ali Ahmed, A.A.E.-M.M., 2012. Using simulation for studying the influence of vertical shading devices on the thermal performance of residential buildings (Case study: New Assiut City). *Ain Shams Eng. J.* 3, 163–174. <https://doi.org/10.1016/j.asej.2012.02.001>.

Al-Kayiem, H.H., Sreejaya, K.v., Gilani, S.I.U.-H., 2014. Mathematical analysis of the influence of the chimney height and collector area on the performance of a roof top solar chimney. *Energy Build.* 68, 305–311. <https://doi.org/10.1016/j.enbuild.2013.09.021>.

Amori, K.E., Mohammed, S.W., 2012. Experimental and numerical studies of solar chimney for natural ventilation in Iraq. *Energy Build.* 47, 450–457. <https://doi.org/10.1016/j.enbuild.2011.12.014>.

Ansys Fluent.co, 2015. ANSYS FLUENT Theory Guide [WWW Document]. URL <http://www.ansys.com/Products/Fluids/ANSYS-Fluent>.

ASHRAE, 2010. Thermal Environmental Conditions for Human Occupancy. American Society of Heating, Refrigerating and Air-Conditioning Engineers.

Attia, S., Evrard, A., Gratia, E., 2012. Development of benchmark models for the Egyptian residential buildings sector. *Appl. Energy* 94, 270–284. <https://doi.org/10.1016/j.apenergy.2012.01.065>.

Attia, S., Gratia, E., De Herde, A., Hensen, J., 2013. Tool for Design Decision Making: Zero Energy Residential Buildings in Hot Humid Climate.

Awbi, H.B., Gan, G., 1992. Simulation of solar-induced ventilation. *Renew. Energy Technol. Environ.* 4, 2016–2030.

Bansal, N.K., Mathur, R., Bhandari, M.S., 1993. Solar chimney for enhanced stack ventilation.

Bolbol, A.A., Fatheldin, A., Omran, M.M., 2005. Financial development, structure, and economic growth: the case of Egypt, 1974–2002. *Res. Int. Bus. Finance* 19, 171–194. <https://doi.org/10.1016/j.ribaf.2004.10.008>.

Bouchair, A., 1994. Solar chimney for promoting cooling ventilation in southern Algeria. *Build. Serv. Eng. Res. Technol.* 15, 81–93. <https://doi.org/10.1177/014362449401500203>.

Calautit, J.K., Hughes, B.R., Chaudhry, H.N., Ghani, S.A., 2013. CFD analysis of a heat transfer device integrated wind tower system for hot and dry climate. *Appl. Energy* 112, 576–591. <https://doi.org/10.1016/j.apenergy.2013.01.021>.

Chen, Q., 1995. Comparison of different k-ε models for indoor air flow computations. *Numer. Heat Transf. Part B Fundam.* 28, 353–369. <https://doi.org/10.1080/10407799508928838>.

Chen, Z.D., Bandopadhyay, P., Halldorsson, J., Byrjalsen, C., Heiselberg, P., Li, Y., 2003. An experimental investigation of a solar chimney model with uniform wall heat flux. *Build. Environ.* 38, 893–906. [https://doi.org/10.1016/S0360-1323\(03\)00057-X](https://doi.org/10.1016/S0360-1323(03)00057-X).

Dabaieh, M., Wanas, O., Hegazy, M.A., Johansson, E., 2015. Reducing cooling demands in a hot dry climate: a simulation study for non-insulated passive cool roof thermal performance in residential buildings. *Energy Build.* 89, 142–152. <https://doi.org/10.1016/j.enbuild.2014.12.034>.

Egyptian Electricity Holding Company-Annual Report 2015/2016 (No. 2015/2016), n.d. . Ministry of Electricity & Renewable Energy, Egypt.

Ennil, A.B., Al-Dadah, R., Mahmoud, S., Rahbar, K., AlJubori, A., 2016. Minimization of loss in small scale axial air turbine using CFD modeling and evolutionary algorithm optimization. *Appl. Therm. Eng.* 102, 841–848. <https://doi.org/10.1016/j.applthermaleng.2016.03.077>.

Gan, G., 2006. Simulation of buoyancy-induced flow in open cavities for natural ventilation. *Energy Build.* 38, 410–420. <https://doi.org/10.1016/j.enbuild.2005.08.002>.

Gan, G., Riffat, S.B., 1998. A numerical study of solar chimney for natural ventilation of buildings with heat recovery. *Appl. Therm. Eng.* 18, 1171–1187.

Haaker, M.P.R., Verheijen, P.J.T., 2004. Local and global sensitivity analysis for a reactor design with parameter uncertainty. *Chem. Eng. Res. Des.* 82, 591–598.

Hamdy, I., Fikry, M.A., 1998. Paasive Solar ventilation. *Renew. Energy* 14, 381–386.

Harris, D.J., Helwig, N., 2007. Solar chimney and building ventilation. *Appl. Energy* 84, 135–146. <https://doi.org/10.1016/j.apenergy.2006.07.001>.

Ho, S.H., Rosario, L., Rahman, M.M., 2009. Thermal comfort enhancement by using a ceiling fan. *Appl. Therm. Eng.* 29, 1648–1656. <https://doi.org/10.1016/j.applthermaleng.2008.07.015>.

Ibrahim, A., 2011. Renewable energy sources in the Egyptian electricity market: a review. *Renew. Sustain. Energy. Rev.* <https://doi.org/10.1016/j.rser.2011.07.149>.

Imran, A.A., Jalil, J.M., Ahmed, S.T., 2015. Induced flow for ventilation and cooling by a solar chimney. *Renew. Energy* 78, 236–244. <https://doi.org/10.1016/j.renene.2015.01.019>.

Jing, H., Chen, Z., Li, A., 2015. Experimental study of the prediction of the ventilation flow rate through solar chimney with large gap-to-height ratios. *Build. Environ.* 89, 150–159. <https://doi.org/10.1016/j.buildenv.2015.02.018>.

Kasaiean, A., Ghalamchi, Mehran, Ghalamchi, Mehrdad, 2014. Simulation and optimization of geometric parameters of a solar chimney in Tehran. *Energy Convers. Manag.* 83, 28–34. <https://doi.org/10.1016/j.enconman.2014.03.042>.

Khanal, R., Lei, C., 2015. A numerical investigation of buoyancy induced turbulent air flow in an inclined passive wall solar chimney for natural ventilation. *Energy Build.* 93, 217–226. <https://doi.org/10.1016/j.enbuild.2015.02.019>.

Khanal, R., Lei, C., 2014. An experimental investigation of an inclined passive wall solar chimney for natural ventilation. *Sol. Energy* 107, 461–474. <https://doi.org/10.1016/j.solener.2014.05.032>.

Khedari, J., Boonsri, B., Hirunlabh, J., 2000a. Ventilation impact of a solar chimney on indoor temperature fluctuation and air change in a school building. *Energy Build.* 32, 89–93.

Khedari, J., Mansirisub, W., Chaima, S., Pratinthong, N., Hirunlabh, J., 2000b. Field measurements of performance of roof solar collector. *Energy Build.* 31, 171–178.

Kumar, S., Sinha, S., Kumar, N., 1998. Experimental investigation of solar chimney assisted bioclimatic architecture. *Energy Convers. Manag.* 39, 441–444. [https://doi.org/10.1016/S0196-8904\(97\)00024-1](https://doi.org/10.1016/S0196-8904(97)00024-1).

Mahdy, M.M., Nikolopoulou, M., 2014. Evaluation of fenestration specifications in Egypt in terms of energy consumption and long term cost-effectiveness. *Energy Build.* 69, 329–343. <https://doi.org/10.1016/j.enbuild.2013.11.028>.

Mathur, J., Bansal, N.K., Mathur, S., Jain, M., Anupma, 2006. Experimental investigations on solar chimney for room ventilation. *Sol. Energy* 80, 927–935. <https://doi.org/10.1016/j.solener.2005.08.008>.

Nicol, F., 2004. Adaptive thermal comfort standards in the hot-humid tropics. *Energy Build.* 36, 628–637. <https://doi.org/10.1016/j.enbuild.2004.01.016>.

- O'Connor, D., Calautit, J.K., Hughes, B.R., 2016. A novel design of a desiccant rotary wheel for passive ventilation applications. *Appl. Energy* 179, 99–109. <https://doi.org/10.1016/j.apenergy.2016.06.029>.
- Ong, K.S., 2003. A mathematical model of a solar chimney. *Renew. Energy* 28, 1047–1060.
- Paliaga, G., 2009. Moving air for comfort. *ASHRAE J.* 51, 18.
- Patel, S.K., Prasad, D., Ahmed, M.R., 2014. Computational studies on the effect of geometric parameters on the performance of a solar chimney power plant. *Energy Convers. Manag.* 77, 424–431. <https://doi.org/10.1016/j.enconman.2013.09.056>.
- Saleem, A.A., Abel-Rahman, A.K., Ali, A.H.H., 2014. Experimental study on thermal comfort conditions in existing public primary schools buildings in Upper Egypt. In: *Sustainability in Energy and Buildings: Research Advances*. Presented at the International Conference on Sustainability in Energy and Buildings- SEB-14, Future Technology Press, Cardiff, Wales, UK, p. 6.
- Saleem, Ahmed A., Abel-Rahman, A.K., Ali, A.H.H., Ookawara, S., 2016a. An analysis of thermal comfort and energy consumption within public primary schools in Egypt. *IAFOR J. Sustain. Energy Environ.* 3.
- Saleem, Ahmed Abdeen, Bady, M., Ookawara, S., Abdel-Rahman, A.K., 2016b. Solar Chimney Design for Standard Ventilation Rate of Residential Buildings in a Hot-Arid Climate. Presented at the 9th International Conference on Indoor Air Quality Ventilation & Energy Conservation In Building, Incheon, South Korea, p. 8.
- Saleem, Ahmed Abdeen, Bady, M., Ookawara, S., Abdel-Rahman, A.K., 2016c. Achieving standard natural ventilation rate of dwellings in a hot-arid climate using solar chimney. *Energy Build.* 133, 360–370. <https://doi.org/10.1016/j.enbuild.2016.10.001>.
- Schiavon, S., Melikov, A.K., 2008. Energy saving and improved comfort by increased air movement. *Energy Build.* 40, 1954–1960. <https://doi.org/10.1016/j.enbuild.2008.05.001>.
- Serageldin, A.A., Abdelrahman, A.K., Ookawara, S., 2016. Earth-air heat exchanger thermal performance in Egyptian conditions: experimental results, mathematical model, and Computational Fluid Dynamics simulation. *Energy Convers. Manag.* 122, 25–38. <https://doi.org/10.1016/j.enconman.2016.05.053>.
- Siva Reddy, V., Premalatha, M., Ranjan, K.R., 2012. Experimental studies on solar chimney for enhanced ventilation. *Int. J. Sustain. Energy* 31, 35–42. <https://doi.org/10.1080/1478646X.2010.534554>.
- Suárez-López, M.J., Blanco-Marigorta, A.M., Gutiérrez-Trashorras, A.J., Pistono-Favero, J., Blanco-Marigorta, E., 2015. Numerical simulation and exergetic analysis of building ventilation solar chimneys. *Energy Convers. Manag.* 96, 1–11. <https://doi.org/10.1016/j.enconman.2015.02.049>.
- Sudprasert, S., Chinsorranant, C., Rattanadecho, P., 2016. Numerical study of vertical solar chimneys with moist air in a hot and humid climate. *Int. J. Heat Mass Transf.* 102, 645–656. <https://doi.org/10.1016/j.ijheatmasstransfer.2016.06.054>.
- Tan, A., Wong, N., 2013. Parameterization Studies of Solar Chimneys in the Tropics. *Energies* 6, 145–163. <https://doi.org/10.3390/en6010145>.
- Tan, A.Y.K., Wong, N.H., 2014. Influences of ambient air speed and internal heat load on the performance of solar chimney in the tropics. *Sol. Energy* 102, 116–125. <https://doi.org/10.1016/j.solener.2014.01.023>.
- Thompson, J., Walton, S., Hassan, O., Rolland, S., Sienz, J., 2017. The use of CFD and multi-objective optimisation techniques to customise an industrial pre-mixer. *Struct. Multidiscip. Optim.* 55, 2339–2351. <https://doi.org/10.1007/s00158-016-1643-7>.
- Yang, W., Zhang, G., 2009. Air movement preferences observed in naturally ventilated buildings in humid subtropical climate zone in China. *Int. J. Biometeorol.* 53, 563–573. <https://doi.org/10.1007/s00484-009-0246-z>.